NUMERICAL SIMULATION OF A CIRRUS CLOUD AND ITS DETECTABILITY BY A CLOUD RADAR

Ken-ichi Maruyama[1)*] , Lubomir Levkov[2)]
and Yasushi Fujiyoshi[3) 1)]
[1)] Frontier Research System for Global Change
[2)] GKSS Research Center
[3)] Institute of Low Temperature Science, Hokkaido Univ.

1. INTRODUCTION

Little observational information for ice water budget might lead to the significant range in GCM results. There are two ways to give more constraints in GCM. The one is to improve information from future satellite mission using mm-radar and other cloud sensors. The other is to improve quantitative physical understanding of the processes of cirrus cloud formation, maintenance and dissipation.(D.Starr, 2000) We intend to contribute to the latter through numerical modeling.

Using profiles from GEWEX GCSS WG2 ICMC (Idealized Cirrus Model Comparison) and a 3D non-hydrostatic model, we investigate the sensitivities of a cirrus cloud model to primary ice nucleation, shortwave and longwave radiation and vertical wind shear.

In addition we also calculated the radar reflectivities of simulated cirrus clouds.

2. GESIMA

2.1 Dynamics

The Geesthacht Simulation Model of the Atmosphere (GESIMA) is three-dimensional and non-hydrostatic. (Levkov et al. 1995, Kapitza and Eppel 1992)

The predicted model variables are the velocity, potential temperature, the mixing ratio for water vapor, the mixing ratios and number concentration for cloud ice, cloud water and rain, and the number concentration for aerosol particles.

The dynamical equations and the equation for the potential temperature are integrated in time by a predictor-corrector scheme. Advection is calculated by MacCormack's scheme(Anderson et al., 1984). All water species are integrated with a simple forward scheme and the advection transport algorithm of Smolarkiewicz (1984) is used. The eddy diffusion terms are calculated by a first order closure according to the level 2.5 in the hierarchy of Mellor and Yamada (1974). The diffusion coefficients are a function of turbulent kinetic energy and are calculated explicitly.

The continuity equations for grid volume average mixing ratio of species X of water (q_X), potential temperature deviation (Θ') and number concentration (N_X) of cloud particles, and number concentration of aerosol particles (N_A) can be written as follows:

$$\frac{\partial q_X}{\partial t} = ADV(q_X) + DIF(q_X) + \frac{\partial}{\partial z}(q_X U_X) + Q_{q_X} \quad (1)$$

$$\frac{\partial \Theta'}{\partial t} = ADV(\Theta') + DIF(\Theta') + Q_{\Theta'} \quad (2)$$

$$\frac{\partial N_X}{\partial t} = ADV(N_X) + DIF(N_X) + \frac{\partial}{\partial z}(N_X U_X) + Q_{N_X} \quad (3)$$

$$\frac{\partial N_A}{\partial t} = ADV(N_A) + DIF(N_A) - N_W \quad (4)$$

The subscripts X stands for cloud water, rain water and vapor. "ADV" represents the advection and "DIF" the eddy diffusion term. U_X is the mass weighted mean velocity for rain drops and Q_{q_X}, Q_{N_X} and $Q_{\Theta'}$ denotes the change of the water species and temperature due to microphysical and radiative processes.

2.2 Microphysics

*Corresponding author address:
Ken-ichi Maruyama, Frontier Research System for Global Change, SEAVANS N7F 1-2-1 Sibaura Minato-ku Tokyo 151-6791, Japan ; E-mail: maruyama@frontier.esto.or.jp

It is recognized that ice in clouds are produced through deposition/condensation freezing nucleation and heterogeneous, homogeneous and contact freezing. There is, however, some uncertainties about the amount of ice active nuclei in each ice nucleation mechanism and its dependence on temperature and supersaturation.

The three microphysics parameterizations were described and tested by Levkov et al.(1992, 1994, 1995). We tested two parameterizations in this study, which are the combination of Cotton(1986) and Young(1974)(hereafter Cotton) and Meyers' (1992).

In Cotton, the deposition/condensation freezing nucleation rate is based on Cotton(1986) and to quantify the ice nucleaton rate from contact freezing Young(1974)'s model is used. Cotton(1986) generalized temperature dependent Fletcher(1962)'s equation to include a supersaturation dependence of Huffman and Vali(1973)'s equation as follows.

$$\overline{m_I}\frac{\partial N_{ID}}{\partial t} = \overline{m_I} N_0 B \left[\frac{S_I - 1}{S_0 - 1}\right]^{b'} \exp\left[\beta_2 (T_0 - T)\right] \tag{5}$$

Young's model is in the form as shown below.

$$\overline{m_I}\frac{\partial N_{IC}}{\partial t} = \overline{m_W} N_a 0 (T_{crit} - T_C)^{1.3} \tag{6}$$

where $N_a 0 = 2 \cdot 10^5 m^{-3}$ and $T_{crit} = 270.16K$. T_C is the absolute cloud droplet temperature which is in this study assumed to be equal to the absolute temperature T of the environment. N_{IC} denotes the predicted number of contact freezing nuclei.

In Meyers, the effects of deposition and condensation freezing are combined in a single expression which predicts the nucleation rate as an exponential function of the supersaturation with respect with ice(Meyers et al.(1992))

$$\overline{m_I}\frac{\partial N_{ID}}{\partial t} = \overline{m_I} * 1000 * \exp\left\{a + b\left[100(S_i - 1)\right]\right\} \tag{7}$$

where a = -0.639 and b = 0.1296

The nucleation rate due to contact freezing is given in the Meyers' case as an exponential function of the temperature

$$\overline{m_I}\frac{\partial N_{IC}}{\partial t} = \overline{m_W} * 1000 * \exp\left\{c + d\left[T_0 - T_c\right]\right\} \tag{8}$$

where c = -2.8 and d = 0.262.

3. SIMULATIONS AND RESULTS

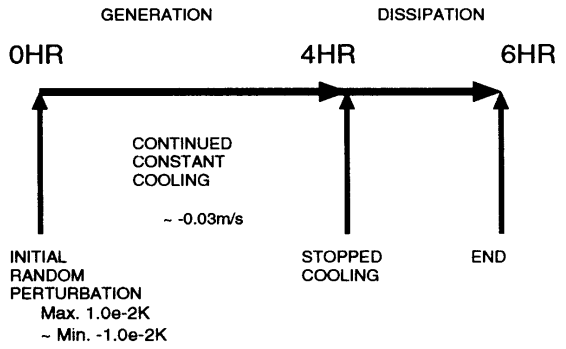

Figure 1: The design of the numerical experiment given by ICMC.

We used the warm neutral case from profiles of GEWEX GCSS WG2 ICMC and a 1D y model for creating an input for a 3D model(fig.2). The design of numerical experiments given by ICMC is shown in fig.1

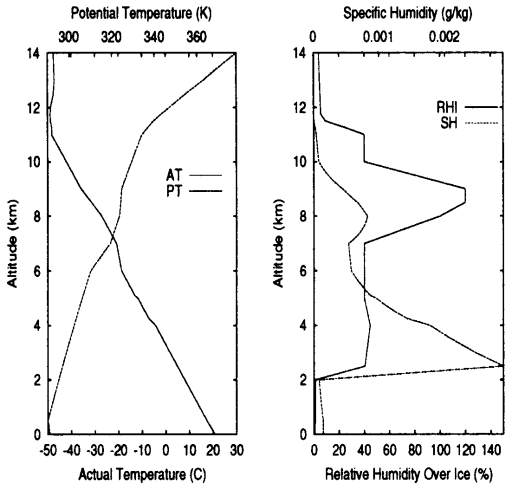

Figure 2: Initial profiles for the warm neutral case

We will show the results from sensitivity tests of the cirrus cloud model to the following effects: shortwave and longwave radiation, parameterization on primary ice nucleation and vertical wind shear.

Here the mesoscale model was run over 10 x 10 km^2 domain. The model resolution was fixed to 250m in the horizontal direction and varied from 100m to 500m in the vertical direction. (Hereafter SW+LW, LW and NO denotes the case including the shortwave and longwave radiation, the case including only the longwave radiation and the case

which includes no radiation respectively.)

In Meyers' cases, while constant cooling continued until 4 hours after the start, the peak value of IWC was gained at about 3 hours. This could be explained by snow falling out and melting. While the maximum of ice mass is located in the upper layer at 180min., it is located in the lower layer at 240 min. as shown in fig.10.

The averages of ice water contents, ice and snow number concentrations are shown as a function of time in fig.3., fig.4 and fig.5 respectively.

In Cottons' cases, IWC of the NO case decreases rapidly compared to other cases. IWC of the SW+LW case starts to decrease at about 1 hour and increase again at about 3 hours and seems to stop to increase after 4 hours, while LW case increases continuously.

Comparing Cotton's cases and Meyers' cases, IWCs of Cotton's cases become higher values at earlier times than Meyers' cases. With Meyers' parameterization, IWC of SW+LW case become larger than that of LW case after 3 hours' simulation, while with Cotton's parameterization, IWC of SW+LW is larger that of LW throughout the simulation.

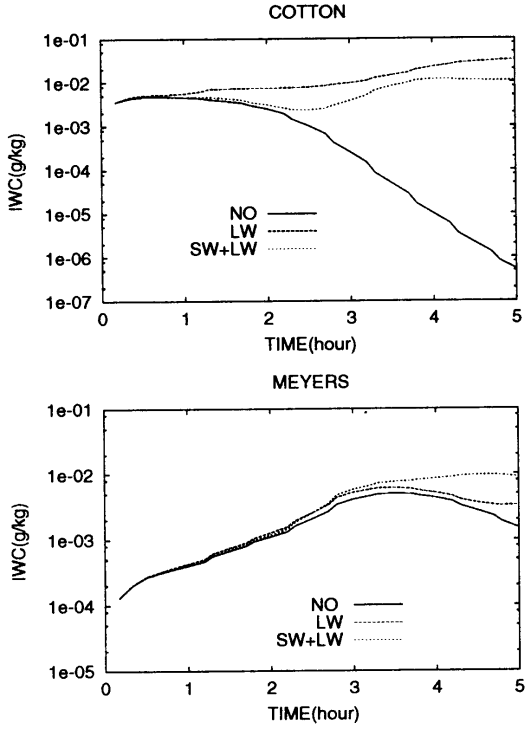

Figure 3: The averages of ice water contents over the whole domain are shown as a function of time for the SW+LW, LW and NO cases of Cotton and Meyers.

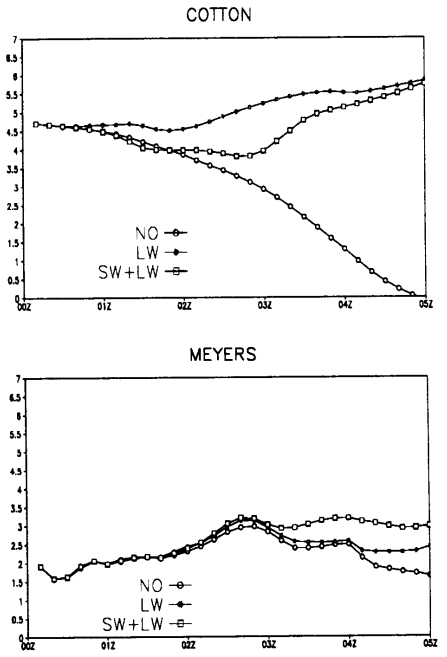

Figure 4: The averages of ice number concentrations ($1/m^3$ in log) over the whole domain are shown as a function of time for the SW+LW, LW and NO cases of Meyers and Cotton.

3.2 The effect of vertical wind shear

We used a 90 $\times$ 10 km^2 domain which is extended along the wind shear direction to avoid the effect of boundary. Then we compared 10 $\times$ 10 km^2 in the center of the domain(see fig.6) with the no shear case. For this case, we used Meyers' parameterization and included only infrared radiation.

Concerning about IWC, the difference between both cases is not very large in the beginning, but in the end of simulation, IWC of the vertical wind shear case is larger than that of the no shear case (fig.7). The structure of the case with the shear is more horizontally homogeneous than that of the case without the shear(fig.10).

4. RADAR REFLECTIVITY

In addition, we calculate the radar reflectivies from simulated cirrus clouds by a 95GHz radar. In the model, pristine ice crystals are assumed to be mono-dispersed and snow crystals are distributed as a Marshall-Palmer distribution. The radar back-scattering crosssection of an ice spherical particle by Mie calculations is shown as a function of particle size in fig.8. Judging from fig.8, unless their particle sizes exceeds about 500

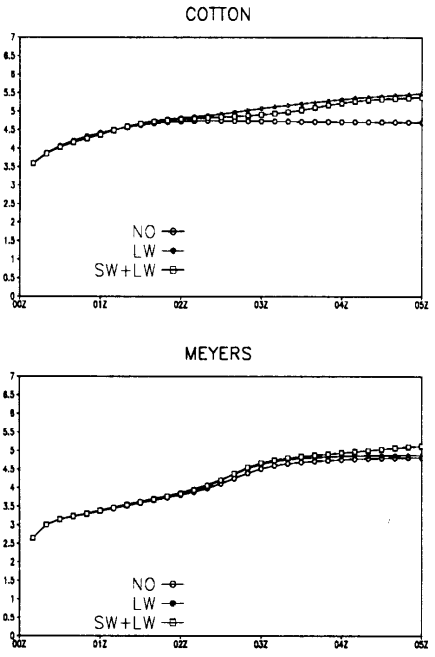

Figure 5: The same as fig.4, but snow number concentration.

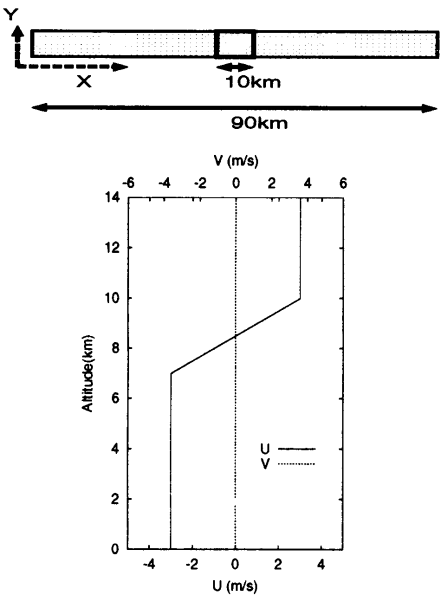

Figure 6: The initial profiles of U and V and the domain for the case with vertical shear.

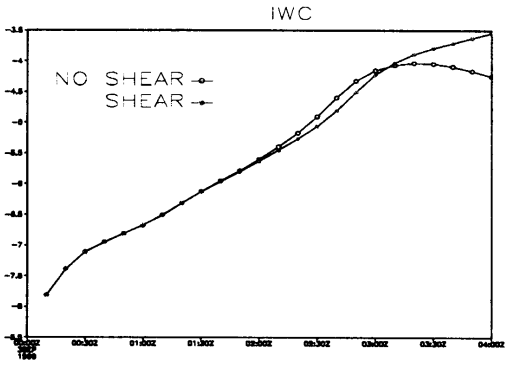

Figure 7: The averaged IWCs are shown as a function of time for the cases with and without shear. Both cases used the Meyers' parameterization and included only infrared radiation.

μm, Rayleigh scattering approximation can be applied. Therefore we calculated radar reflectivities by 95GHz radar according to the following equation (see also Murakami(1990)).

$$dBZ = 10 \log Z, \tag{9}$$

where

$$Z = N_I \left(\frac{6\bar{\rho} Q_I}{N_I \rho_I} \right)^6 \frac{K_i^2}{K_w^2} \left(\frac{\rho_i}{\rho_w} \right)^2 * 10^{18}$$

$$+\Gamma(7) \frac{K_i^2}{K_w^2} \left(\frac{\rho_s}{\rho_w} \right)^2 N_{s0} \left(\frac{\bar{\rho} Q_s}{\pi \rho_s N_{s0}} \right)^{1.75} * 10^{18} \tag{10}$$

$$K_i^2 = \left| \frac{\epsilon_i - 1}{\epsilon_i + 2} \right|^2, \quad K_w^2 = \left| \frac{\epsilon_w - 1}{\epsilon_w + 2} \right|^2,$$

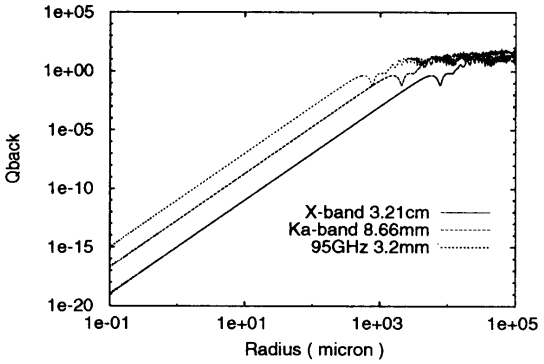

Figure 8: The radar backscattering cross section of a spherical ice(λ = 3.21cm, 8.66mm and 3.2mm) is shown as a function of its radius.

where ϵ_i and ϵ_w are the dielectric constants of ice and water, ρ_i, ρ_w,ρ_s and $\bar{\rho}$ are densities of ice, water, snow, and air respectively.

In Cotton's case, it is seen that LW and LW+SW cases have small peaks around 1.5 hour and LW+SWcontent and radar reflectivity) are significant. has a peak around 4 hours after the start (fig.9 upper panel). Compared to IWC, the first small peaks appears about 1 hour later. This could be related to sizes of particles contained in simulated clouds and the dependence of radar backscattering crosssections on the radius of an ice particle.

In Meyers' case, LW and SW+LW cases have maximum values around 3 hours(fig.9 lower panel).

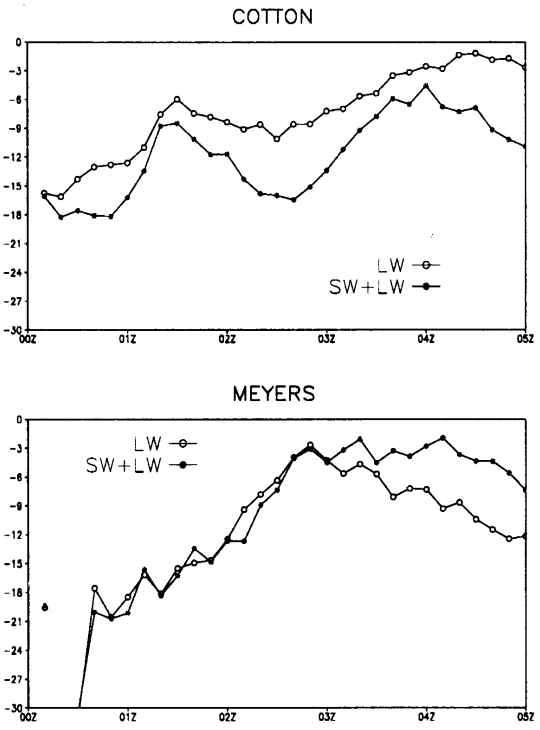

Figure 9: The averages of the radar reflectivity (dBZ) over the whole domain are shown as a function of time for the LW and SW+LW cases of Cotton(upper panel) and Meyers(lower panel).

5. CONCLUDING REMARKS

Using GEWEX GCSS WG2 ICMC profiles and a 3D non-hydrostatic model GESIMA, we simulated cirrus clouds numerically and examined model sensitivities to several physical conditions, such as ice microphysics parameterizations, longwave and shortwave radiation and vertical wind shear.

We tested two different ice microphysics parameterizations for the cases which include shortwave and longwave radiation, the cases which include only longwave radiation and no radiation

In the case of Meyers' parameterization, almost 3 hours later, IWC of the full radiation case increases more than that of the only infrared radiation case, while in the case of Cotton's, IWC of the only infrared radiation case is larger than the of the full radiaton case throughout the simulation.

Cirrus clouds in the vertical wind shear case became more horizontally homogeneous than those in the no shear case. IWC in the shear case, in the end of simulation, become larger than that of the no shear case.

References

[1] Kapieta, H. and Eppel, D.P. The non-hydrostatic mesoscale model GESIMA. Part I: Dynamical equations and tests . *Contrib. Atmos. Phys.*, 65:129–145, 1992.

[2] Levkov, L., Boin, M., and Rockel, B. Impact of primary ice nucleation parameterizations on the formation and maintenance of cirrus. *Atmos. Res.*, 38:147–159, 1995.

[3] Levkov, L., Rockel, B., Kapieta, H., and Raschke, R. 3D mesoscale numerical studies of cirrus and stratus clouds by their time and space evolution. *Contrib. Atmos. Phys.*, 65:35–58, 1992.

[4] Murakami, M. Numerical modeling of dynamical and microphysical evolution of an isolated convective cloud. *J.Meteo.Soc.Japan*, 68:398–414, 1990.

[5] Starr, D. GEWEX Cloud System Study Working Group II - Cirrus Cloud Systems 1999 Report. 2000.

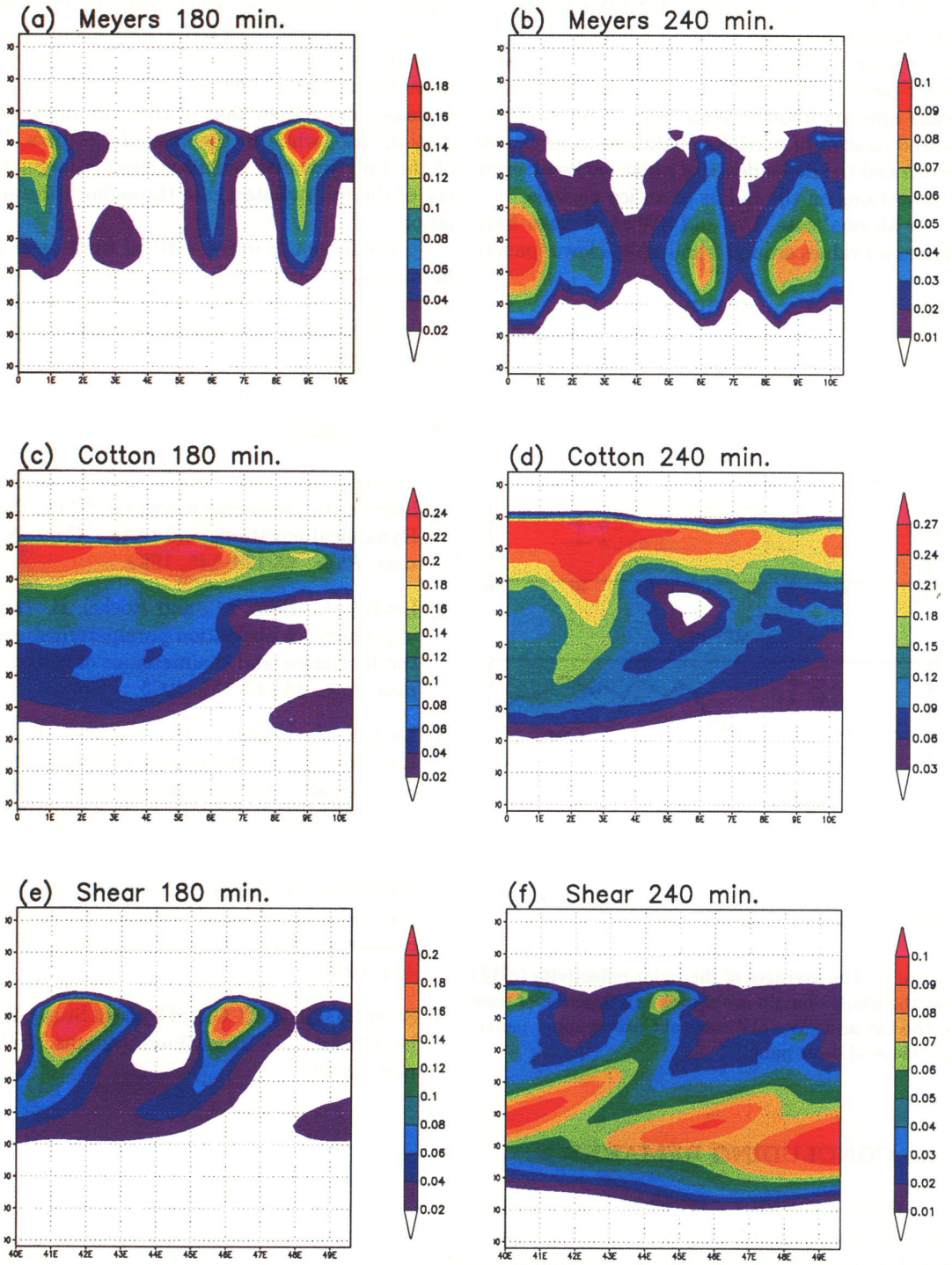

Figure 10: The vertical cross sections (at y = 4km) of QI and QS(g/kg) are shown for the case of Meyers at (a) 180min. , (b) 360min. , for the case of Cotton at (c) 180min. and (b) 240min. and for the Meyers' case with vertical wind shear at (e) 180min. and (f) 240min. All cases in this figure include only longwave radiation.